A Directly Matched PA-Integrated K-band Antenna for Efficient mm-Wave High-Power Generation

(article starts on next page)

A Directly Matched PA-Integrated K-band Antenna for Efficient mm-Wave High-Power Generation

Wan-Chun Liao, *Student Member, IEEE,* Rob Maaskant, *Senior Member, IEEE,*
Thomas Emanuelsson, *Member, IEEE,* Vessen Vassilev, *Member, IEEE,* Oleg Iupikov, *Member, IEEE,*
and Marianna Ivashina, *Senior Member, IEEE*

Abstract—A K-band slot antenna element with integrated GaN (gallium nitride) power amplifier (PA) is presented. It has been optimized through a circuit-EM co-design methodology to directly match the transistor drain output to its optimal load impedance ($Z_{\mathrm{opt}} = 17 + j46\,\Omega$) while accounting for the over-the-air coupling effects in the vicinity of the transition between the PA and antenna. This obviates the need for using a potentially lossy and bandwidth-limiting output impedance matching network. The measured PA-integrated antenna gain of 15 dBi with a 40% total efficiency at 28 dBm output power agrees well with the theoretically achievable performance targets. The proposed element is compact ($0.6 \times 0.5 \times 0.3\,\lambda^3$), and thus well-suited to meet the high-performance demands of future emerging beamforming active antenna array applications.

Index Terms—millimeter-wave antennas, gallium nitride (GaN), active integrated antennas, power amplifiers, antenna-circuit co-design, K-band, antenna array element.

I. INTRODUCTION

THE forthcoming demands on high capacity and data throughput in wireless communication systems are unable to be fulfilled by conventional sub-6 GHz bands [1]. Conversely, mm-wave power amplifier integrated active antenna (PAIAA) designs can offer an improved performance, be potentially low-cost and of compact size [2]–[4]. These PAIAAs are therefore promising candidates to constitute the next-generation antenna technology.

Previous studies of PAIAA designs in the S- and C-bands have been conducted in [5]–[9]. In [8], a GaN high electron mobility transistor (HEMT) was used in the power amplifier design achieving a maximum output power of 38 dBm and a maximum power-added efficiency (PAE) of 59% in C-band, in which the PA and antenna are interconnected through a harmonic tuning and impedance matching network. Albeit that the design in [8] has good thermal capabilities, its size is rather bulky ($1.9 \times 1.9 \times 2.1\,\lambda^3$). In [9] a W-band PA-antenna integrated design in silicon technology was reported, which

W.-C. Liao, O. Iupikov and M. Ivashina are with the Department of Electrical Engineering, Chalmers University of Technology, 41296 Gothenburg, Sweden (e-mail:liao@chalmers.se).

R. Maaskant is with the Department of Electrical Engineering, Chalmers University of Technology, 41296 Gothenburg, Sweden, and also with the Department of Electrical Engineering, Eindhoven University of Technology, 5612 AZ Eindhoven, The Netherlands.

T. Emanuelsson is with the Microwave Electronics Laboratory, Chalmers University, 41296 Gothenburg, Sweden, and also with Gapwave AB, 41451 Gothenburg, Sweden.

V. Vassilev is with the Microwave Electronics Laboratory, Chalmers University of Technology, 41296 Gothenburg, Sweden.
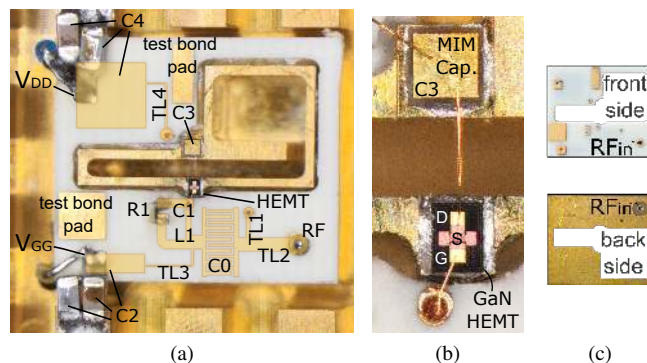
Fig. 1. Antenna integration approach employing direct impedance matching to the PA without intermediate impedance matching circuitry: (a) A K-band PA-Integrated active b-shaped slot antenna on a ground plane comprising a bed of nails (dimensions: 9.1 mm $\times$ 7.3 mm). Translucent parts embedded in the substrate. (b) The drain of the Qorvo GaN HEMT die is directly integrated over the radiating slot and bonded to the Tecdia MIM (Metal-Insulator-Metal) capacitor as depicted in Fig. 2. (c) Front- and back-side of PCB.

is much more compact ($0.4 \times 0.4\,\lambda^2$), though its peak PAE is merely 6.4% and the equivalent isotropic radiated power (EIRP) along the on-axis direction is about 3 dBm.

Among the plethora of studies on PAIAAs, there is a lack of PA-antenna co-design methodologies for achieving optimal active integrated antenna designs that account accurately for both nonlinear and antenna coupling effects. An initial design flow for integrated active antennas (IAAs) in the mm-wave frequency range has been presented in [10], in which the first iteration of the co-optimization method was discussed. The present paper elaborates on the co-design methodology by introducing a combined electromagnetics (EM)-circuit multiport analysis to co-optimize the integrated design. The over-the-air coupling (antenna feedback) effects and nonlinear PA behavior are taken into consideration. This has led to a relatively low-cost, compact, high efficiency, and high output power integrated antenna element design for array antenna systems exhibiting very good thermal handling capabilities.

One major design challenge is to determine the optimal PA-antenna interface impedance. On the one hand, high-power PAs typically prefer a low optimal load resistance (limited by the breakdown voltage of the transistor technology) and an inductive optimal load reactance for maximum efficiency and output power; on the other hand, the antenna input resistance is typically relatively high for attaining high radiation efficiency, such as $50\,\Omega$ or $75\,\Omega$, which are the common characteristic impedances of transmission lines. The optimum load impedance of the two sub-systems are

profoundly distinct and therefore it is improbable to have an optimum impedance that can attain the peak performance for both sub-systems. Ergo, a trade-off study is needed to determine the optimal interface impedance that will lead us to the targeted design goals.

II. ANTENNA-PA CO-DESIGN METHODOLOGY

A. Performance Metrics

In this study we define the key target design goals as [10]:
- Output power per element: $15\,\mathrm{dBm}$ to $25\,\mathrm{dBm}$
- Total power efficiency: $>25\,\%$
- Instantaneous (real-time) bandwidth: $1\,\%$–$5\,\%$ at $20\,\mathrm{GHz}$

B. General Design Flow

The key steps in the design flow are as proposed in [10], where our choice of the integration level at this stage is to use a transistor-on-chip and to design the remaining circuitry off-chip as part of the radiating antenna element:

1) Choice of transistor and load-pull: GaN is a popular semiconductor material for mm-wave integrated circuits (ICs) whenever a relatively high peak output power is required [1], [11]. The choices of commercially available transistors are limited by their technologies and the targeted design frequency range. The Qorvo TGF2942 GaN HEMT was selected on account of its high output power and the availability of the Modelithics transistor model compatible with Keysight's ADS circuit solver [12]. Simulated load-pull data was utilized to find the optimal PA load impedance for maximum output power and PAE. The optimal load resistance was found to be relatively low ($17\,\Omega$) and connected in series with an inductor having a reactance of $46\,\Omega$ to yield a $55\,\%$ PAE. One should synthesize this impedance through proper antenna design in the case a direct PA-antenna impedance match is desired (no output impedance matching network). Simulations show $10\,\%$ average improvement on the PAE for a directly impedance-matched situation relative to the case of a lossy $50\,\Omega$ RO4350B [13] microstrip-line stub-based impedance matching network. Results are omitted due to limited space.

2) Choice of antenna element: The antenna is electrically small so that it can be used as an antenna array element. Furthermore, it was selected to offer an input impedance with low resistance and an inductance such as to directly match it to the aforementioned optimal load impedance. This obviates the need for using an output matching network, which not only reduces power dissipation but also increases both the efficiency and the total radiated power. Finally, heat dissipation is an important issue in PAIAA designs. A metal-only antenna eases the thermal power management as it serves as a heat sink, which is also beneficial for the antenna radiation efficiency; the radiation efficiency was simulated to be 78–$90\,\%$ in the 19–$21\,\mathrm{GHz}$ range.

3) Co-optimization: In this step the characteristics of the PAIAA design were jointly optimized through the combined EM/circuit analysis approach (cf. Sec. II-D). The schematic of the PAIAA design is shown in Fig. 2, in which the radiating element is directly integrated and matched to the PA via a bondwire connection across the slot antenna, which can also

be seen in Fig. 1. The surrounding circuitry includes the DC-bias lines, the stability circuit, and the input impedance matching network, which are common circuit blocks in amplifier designs.
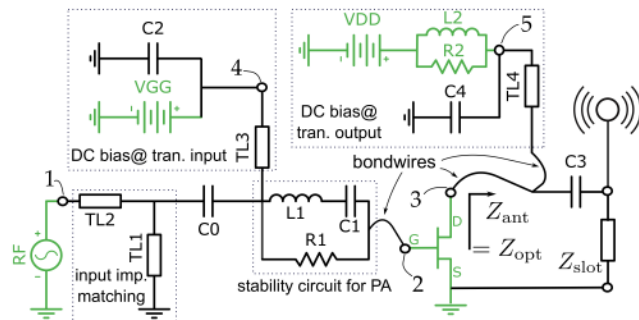

Fig. 2. The schematic of the proposed active integrated antenna design providing a direct optimal impedance match to the PA to maximize the efficiency while obviating the use of (a lossy) impedance matching network as employed conventionally in e.g. [8]. The transistor chip is integrated and connected via a bondwire over the radiating slot. Green components were implemented in the circuit solver; the others were simulated in the full-wave EM solver.

C. Harmonic Termination

The peak efficiency and the fundamental output power of PAs are affected by second and third harmonic drain waveform shaping [14], [15], of which the efficiency can be treated as a function of the second and third harmonic impedance. In general, the peak efficiency requires harmonic shorts or opens at the output of amplifier to generate pure sinusoidal output voltage and current waveforms [14]. In this work, the antenna impedance at the second harmonic shows $|\Gamma_D(2f_o)| \geq 0.96$ and $\angle\Gamma_D(2f_o)$ within $22.5°$ of an open circuit; at the third harmonic the antenna impedance is $|\Gamma_D(3f_o)| \geq 0.95$ and $\angle\Gamma_D(3f_o)$ within $50°$ of an open circuit. A peak efficiency of $49.5\,\%$ can be theoretically achieved with this harmonic termination.

D. Combined EM-Circuit Simulation/Analysis

In Fig. 2 the RF/DC sources and the transistor model (in green) are numerically analyzed in ADS while the rest of the circuitry, i.e., the PCB layout and the radiating element, are analyzed in the combined EM/circuit solver HFSS/ADS. Typically, there is only one port per antenna element in a passive antenna design to represent the excitation port. For PAIAA designs, however, multiple ports per antenna are required to analyze the radiating element and the integrated active device. It is indispensable to have an accurate analysis of the coupling mechanism between all the inter-element ports since, as the element is used in an antenna array, coupling may exist between these ports. This is more complicated than passive antenna arrays due to that the reflected or coupled waves alter the amplifier load impedance and thereby the amplifier characteristics, or give rise to undesired feedback effects possibly affecting the system stability [16].

A design flow between the circuit and EM solvers was proposed in [10], which described the co-optimization procedure for PAIAA systems. In this work, the circuit/EM solvers are interconnected by five single-mode ports between the circuit schematic (Fig. 2) and the EM model (Fig. 3).

Multiple iterations are required to realize a co-optimized PAIAA design, such as adjusting the DC-bias for the PA to improve the PAE and modifying the antenna to increase its radiation efficiency without compromising the PAE.

The PA in the integrated co-design concept in [9] was assumed as a metallic plate in the EM solver, thereby neglecting the dielectric effect and approximating the over-the-air coupling behavior in the vicinity of the transition between the PA and the dipole antenna. In this work, the substrate, the bonding pads, and the metallic ground of the transistor chip are included in the EM model. In addition, the bondwires are included in the numerical model, one of which is used for exciting the radiating element (via the drain pad) and the other two are used to interconnect to the other circuitry components in the EM model (Fig. 1). It is worth mentioning that, ideally, one would EM-model the linear/passive material of the die and have a circuit model of the on-chip transistor excluding this material effect to not account for it twice. Also, it is assumed that the Modelithics FET models are also adequate in our specific EM packaging environment. Thus, a more accurate modeling approach remains a subject of future studies.

III. PROPOSED PA-INTEGRATED ANTENNA DESIGN

The proposed PAIAA element consist of a multilayer printed circuit board (PCB) for the PA circuitry and a metallic radiating structure. A metal-only antenna has been chosen as the radiating structure for its high radiation efficiency and great thermal handling capabilities (heat sink functionality). To enable a direct PA-antenna impedance match, a cavity-backed slot antenna was selected. Furthermore, a stub ($W_3 \times L_3 \times H_2$) was appended to the end of the slot ($W_4 \times L_2 \times H_2$) as seen in Fig. 3(a). The seven impedance tuning parameters are $H_2, L_2, L_3, L_4, W_2, W_3, W_4$, whose values are listed in Table I, where $L_1 \times W_1 \times H_1$ indicates the antenna element dimensions.

The Rogers RO4350B multilayer PCB/laminate has good electrical properties at high frequencies and is relatively low-cost. Except for the lumped components, all of the PA circuitry is printed on the PCB. The PCB layout and the five ports of the design are depicted in Fig. 3(b). The entire PCB has been soldered onto the heat sink for better thermal conduction.

IV. RESULTS

A. Measurement & Calibration Setup

The measurement of a passive antenna is dissimilar from the measurement of an active antenna, in which the RF in- and output powers (at the fundamental and harmonic frequencies) as well as the DC power are all crucial characterization parameters. An illustration of the measurement setup and the reference planes is depicted in Fig. 4. The PAIAA was connected to an Agilent E8363B PNA network analyzer, and

DC-powered by a Rohde & Schwarz HMP4040 power supply. A pre-amplifier was used to increase the input power to the desired range.

The characterization of the PAIAA was conducted in an anechoic chamber. Different from conventional integrated designs where the PA and the antenna can be characterized independently, the transistor die is directly integrated with the antenna forming the device under test (DUT) (Fig. 1); consequently, the antenna and the PA of the DUT have to be characterized concurrently, which increases the complexity of the measurement.

The characterization procedure consists of two measurements. In the first—calibration—measurement (Fig. 4a) the "path gain" G_{path} is measured, which includes all gains/losses, but excludes the known reference antenna gain ($G_{\mathrm{ref.ant}}$ highlighted region between ref. plane B and C):

$$G_{\mathrm{path}} = |S_{21}|^2_{\mathrm{ref}} / G_{\mathrm{ref.ant}} \qquad (1)$$

where $|S_{21}|^2_{\mathrm{ref}}$ is the measured transmission coefficient between the PNA ports (reference plane A and D). In the second measurement (Fig. 4b) the reference antenna is replaced with the DUT, whose active antenna gain is obtained from

$$G_{\mathrm{PA}} \eta_{\mathrm{rad}} D_{\mathrm{ant}} = |S_{21}|^2 / G_{\mathrm{path}} \qquad (2)$$

where G_{PA} is the PA gain, η_{rad} is the antenna radiation efficiency, and D_{ant} is the antenna directivity, which is determined by measuring the radiation pattern over the whole angular space, and $|S_{21}|^2$ is the measured transmission coefficient between the PNA ports for the DUT measurement setup. Hence, the PA gain together with the antenna radiation efficiency is obtained by

$$G_{\mathrm{PA}} \eta_{\mathrm{rad}} = |S_{21}|^2 / (G_{\mathrm{path}} D_{\mathrm{ant}}). \qquad (3)$$

For the efficiency measurement additional knowledge of the DC power (P_{DC}) and the radiated power (P_{out}) at the reference plane E is required. While P_{DC} is measured directly, P_{out} is calculated by knowing the available power from the PNA, the cable loss, the gain of the pre-amplifier, and the PA gain in addition to the radiation efficiency of the DUT.

B. Measurement Result

The PA gain including the radiation efficiency, $G_{\mathrm{PA}} \eta_{\mathrm{rad}} = P_{\mathrm{out}} / P_{\mathrm{acc}}$, is plotted in Fig. 5. An average PA gain of $8\,\mathrm{dB}$,

TABLE I
GEOMETRICAL PARAMETERS (UNIT: mm)

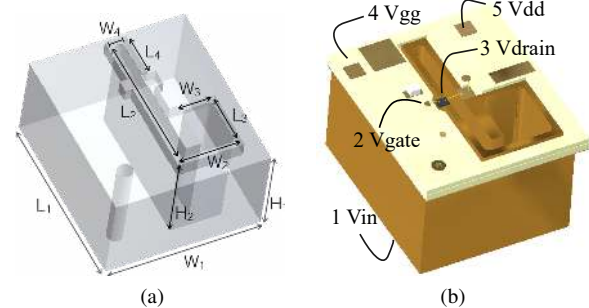| L_1	L_2	L_3	L_4	W_1	W_2	W_3	W_4	H_1	H_2
9.1	7.3	3.1	3.2	7.5	3.4	2.2	0.6	5.4	5.0

(a)   (b)

Fig. 3. (a) The geometry of the proposed PAIAA design; the design parameters are listed in Table I. (b) Five ports of the PAIAA model used in the co-design are denoted: V_{in}, V_{gate}, V_{drain}, V_{gg}, V_{dd} and correspond to the ports in Fig. 2.

TABLE II
PERFORMANCE COMPARISON OF STATE-OF-THE-ART POWER AMPLIFIER-INTEGRATED ACTIVE ANTENNAS

	No output MNK[‡]	Thermal handling	Transistor Technology	Frequency	$P_{1dB,out}$	EIRP	PAE peak	Dimensions $L \times W \times H$, [λ^3]
[8]		great[*]	GaN HEMT	5.8 GHz	38 dBm	44.6 dBm	59.93 %	$1.9 \times 1.9 \times 2.1$
[17]	✓	poor	SiGe HBT	24 GHz	5.6 dBm	4.6 dBm	N/A	$0.2 \times 0.1 \times$ N/A
[18]	✓	poor	0.18 μm CMOS	24 GHz	N/A	N/A	25.6 %	$0.3 \times 0.2 \times$ N/A
[19]	✓	poor	GaAs pHEMT	35 GHz	N/A	N/A	N/A	$0.8 \times 0.8 \times$ N/A
[20]		poor	BiCMOS	60 GHz	12.8 dBm	9.5 dBm	N/A	$0.2 \times 0.2 \times$ N/A
[9]	✓	poor	BiCMOS	79 GHz	19 dBm	3 dBm	11 %[†]	$0.4 \times 0.4 \times$ N/A
This work	✓	good	GaN HEMT	20 GHz	24.7 dBm	30.7 dBm	34.8 %	$0.6 \times 0.5 \times 0.3$

[*]installed on a Peltier unit [†]numerically simulated result [‡]matching network

(a) calibration with the reference antenna
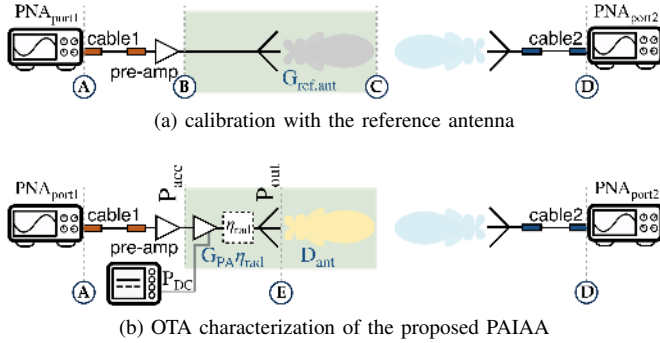

(b) OTA characterization of the proposed PAIAA

Fig. 4. OTA characterization setup in an anechoic chamber

including the radiation efficiency, is observed from 19.5 GHz to 20 GHz. The gain at 20 GHz is about 9 dB showing good agreement with the combined EM-Circuit numerical result.
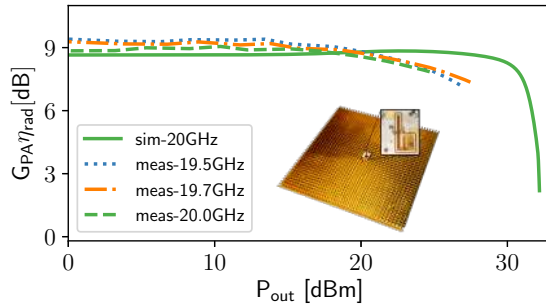

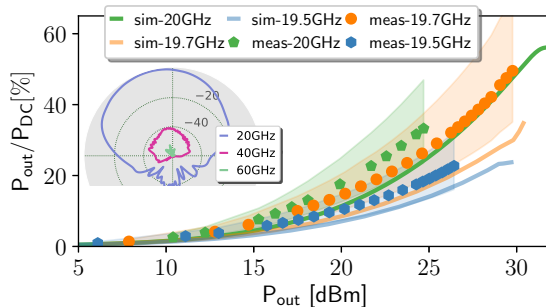Fig. 5. The PA gain including the antenna radiation efficiency at reference plane E (see Fig. 4).

Fig. 6. The efficiency and measurement uncertainty (± 1.5 dB) at the fundamental frequency embedded with the numerical results of second and third harmonics radiation (40 dB lower than at the fundamental frequency).

The efficiency is shown in Fig. 6, in which the measurement uncertainty of ± 1.5 dB is also depicted. The uncertainties are mainly caused by the measurement environment, such as the probe misalignment, reflection in the chamber, and

tolerances on the path loss and reference antenna gain. Note that the frequency shift in the measurement results is due to manufacturing and assembly tolerances. The radiation patterns at 19 GHz and 20 GHz are shown in Fig. 7. A good agreement with the numerical result is observed. At 19.7 GHz, the PAIAA gain ($G_{PA}G_{ant}$) is about 15 dBi, the plot of which is omitted due to space constraints. The simulations indicate that the radiation of the second harmonic is already 40 dB lower than at the fundamental frequency (see Fig. 6).
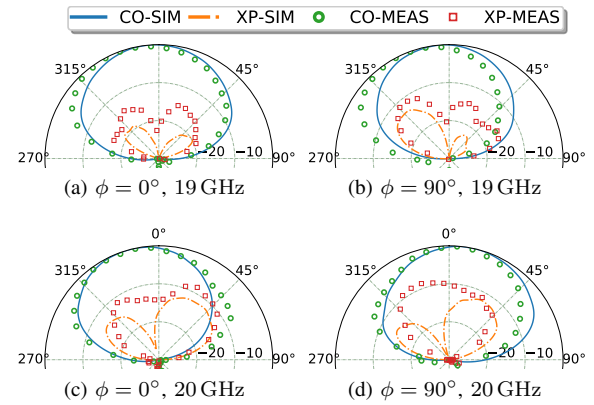

Fig. 7. Normalized radiation pattern at 19 GHz on (a) $\phi = 0°$ and (b) $\phi = 90°$, and at 20 GHz on (c) $\phi = 0°$ and (d) $\phi = 90°$.

V. CONCLUSION

A comparison of our design with state-of-the-art PAIAA design has revealed an efficiency and EIRP comparable to the integrated design in C-band [8], yet with a considerably smaller electrical size. Due to the tolerances on PCB fabrication, CNC milling, and assembly, the optimum input impedance match was shifted to 19.7 GHz, and consequently the maximum radiated power, PA-integrated active antenna gain, and efficiency all occurred at this frequency. An average amplifier gain of 8 dB is observed from 19 GHz to 20 GHz [instantaneous bandwidth: 19.85 GHz $\pm$ 0.15 GHz]. The PA gain and the radiation characteristics both are in good agreement with the combined EM-Circuit numerical result. The PAIAA gain is approximate 15 dBi at 19.7 GHz. The proposed design has demonstrated that high efficiency and high output power PAIAAs can be achieved by using the direct impedance matching technique in conjunction with the proposed co-optimization methodology. The thermal dissipation management is alleviated by using a metal-only antenna, which is compact in size and usable in actively beamformed antenna arrays.

REFERENCES

[1] Ericsson, "On mm-wave technologies for NR (New Radio)," Tech. Rep. R4-164226, 2016.

[2] J. Lin and T. Itoh, "Active Integrated Antennas," *IEEE. Trans. Microw. Theory Tech.*, vol. 42, no. 12, pp. 2186–2194, 1994.

[3] S. Gupta, P. K. Nath, A. Agarwal, and B. K. Sarkar, "Integrated Active Antennas," *Iete Tech. Rev.*, vol. 18, no. 2-3, pp. 139–146, 2001.

[4] K. Chang, R. A. York, P. S. Hall, and T. Itoh, "Active Integrated Antennas," *IEICE Trans. Commun.*, vol. 50, no. 3, pp. 937–944, 2002.

[5] Y. Qin, S. Gao, and A. Sambell, "Broadband High-Efficiency Circularly Polarized Active Antenna and Array for RF Front-End Application," *IEEE Trans. Microw. Theory Tech.*, vol. 54, no. 7, pp. 2910–2916, 2006. [Online]. Available: http://ieeexplore.ieee.org/document/1650428/

[6] Y. Chung, C. Y. Hang, S. Cai, Y. Qian, C. P. Wen, K. L. Wang, and T. Itoh, "AlGaN/GaN HFET Power Amplifier Integrated With Microstrip Antenna for RF Front-End Applications," *IEEE Trans. Microw. Theory Tech.*, vol. 51, no. 2 II, pp. 653–659, 2003.

[7] C. Y. Hang, W. R. Deal, Y. Qian, and T. Itoh, "High-Efficiency PushPull Power Amplifier Integrated with Quasi-Yagi Antenna," *IEEE Trans. Microw. Theory Tech.*, vol. 49, no. 6, pp. 1155–1161, 2001.

[8] N. Hasegawa and N. Shinohara, "C-Band Active-Antenna Design for Effective Integration With a GaN Amplifier," *IEEE Trans. Microw. Theory Tech.*, pp. 1–8, 2017. [Online]. Available: http://ieeexplore.ieee.org/document/7976322/

[9] N. Demirel, Y. Pinto, C. Calvez, D. Titz, C. Luxey, C. Person, D. Gloria, D. Belot, D. Pache, and E. Kerherve, "Codesign of a PA-Antenna Block in Silicon Technology for 80-GHz Radar Application," *IEEE Trans. Circuits Syst. II Express Briefs*, vol. 60, no. 4, pp. 177–181, 2013.

[10] W.-C. Liao, R. Maaskant, T. Emanuelsson, M. Johansson, A. Höök, J. Wettergren, M. Dieudonne, and M. V. Ivashina, "A Ka-Band Active Integrated Antenna for 5G Applications: Initial Design Flow," in *2nd URSI AT-RASC*. IEEE, may 2018. [Online]. Available: https://ieeexplore.ieee.org/document/8471330/

[11] Ericsson, RUAG, SAAB, and Keysight, "Emerging Applications and Systems Employing mm-Wave Frequency Integrated Antenna Arrays," Ericsson, RUAG, SAAB, Keysight, Tech. Rep., 2017.

[12] Keysight Technologies Advanced Design System (ADS) https://www.keysight.com/en/pc-1297113/advanced-design-system-ads.

[13] John Coonrod, Rogers Corporation, Advanced Circuit Materials Division, "Selecting PCB Materials for High-Frequency Applications," *Microw. Eng. Eur.*, no. March/April, pp. 18–21, 2012.

[14] M. Roberg and Z. Popović, "Analysis of High-Efficiency Power Amplifiers With Arbitrary Output Harmonic Terminations," *IEEE Trans. Microw. Theory Tech.*, vol. 59, no. 8, pp. 2037–2048, 2011.

[15] F. H. Raab, "Based Upon a Finite Number of Harmonics," *IEEE Trans. Microw. Theory Tech*, vol. 49, no. 8, pp. 1462–1468, 2001.

[16] M. Ivashina, "Joint Design and Co-integration of Antenna-IC Systems," in *13th European Conference on Antennas and Propagation, (EuCAP 2019)*, April 2019.

[17] E. Öjefors, E. Sönmez, S. Chartier, P. Lindberg, C. Schick, A. Rydberg, and H. Schumacher, "Monolithic Integration of a Folded Dipole Antenna With a 24-GHz Receiver in SiGe HBT Technology," *IEEE Trans. Microw. Theory Tech.*, vol. 55, no. 7, pp. 1467–1474, 2007.

[18] Y. C. Chen, H. H. Chen, T.-G. Ma, and K.-Y. Lin, "K-band Active Antenna Integrated With CMOS Adaptive-bias Power Amplifier," *Proc. 2015 IEEE 4th Asia-Pacific Conf. Antennas Propagation, APCAP 2015*, pp. 427–428, 2016. [Online]. Available: http://ieeexplore.ieee.org/document/7374434/

[19] Y. Song, Y. Wu, J. Yang, Y. Tian, W. Tong, Y. Chen, C. Wang, X. Tang, J. Benedikt, and K. Kang, "A Compact Ka-Band Active Integrated Antenna With a GaAs Amplifier in a Ceramic Package," *IEEE Antennas Wirel. Propag. Lett.*, vol. 16, pp. 2416–2419, 2017.

[20] C.-H. Wang, Y.-H. Cho, C.-S. Lin, H. Wang, C.-H. Chen, D.-C. Niu, J. Yeh, C.-Y. Lee, and J. Chern, "A 60GHz Transmitter with Integrated Antenna in 0.18μm SiGe BiCMOS technology," *ISSCC*, vol. 52, no. 2, pp. 305–312, 2006.